Applied Mathematical Biosystems, Volume 2, Issue 1, (Jan-Jun 2026), 26-37

Applied Mathematical Biosystems

journal homepage: https://ambjournal.com

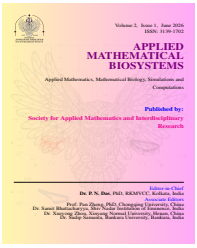

Investigating the glucose metabolism regulatory network through a Caputo fractional order differential model

Vaibhab Ghosh[1]

[1]*Department of Mathematics, Ramakrishna Mission Vivekananda Centenary College, Rahara, Kolkata-700118, West Bengal, India*

Abstract

To model memory-dependent systems, Caputo's fractional-order differentiation has emerged as a predominant framework within the scientific community. From prey-predator networks to complex disease dynamics in eco-epidemiology, fractional-order models represent a robustly analyzed field. Diabetes, a non-communicable metabolic disorder, exhibits dynamics that are critically dependent on long-term systemic behavior. In this study, a fractional-order model is developed and analyzed to interpret the long-term glucose metabolism regulatory network. The model incorporates four state variables: plasma glucose (G), insulin concentration (I), liver glycogen concentration (X), and glucagon concentration (P). The findings have been validated against similar modeling studies and close agreement in the results have been found. Numerical simulations reveal rich dynamical behavior, including stable steady states, damped oscillations, and bifurcation phenomena such as Hopf and transcritical bifurcations. The fractional order (α) is shown to play a crucial role in governing system dynamics, where intermediate values yield results that are most physiologically consistent. This study can potentially provide valuable insights into the long-term behavior of the diabetic pathway, thereby improving the understanding of complex glucose metabolism and its underlying regulatory mechanisms. From a clinical perspective, the proposed framework may aid in evaluating the effects of high-glucose diets and complementary insulin therapies on overall pancreatic health, as reflected through variations in glycogen and glucagon concentrations.

Keywords: *Glucose-regulation, Glycogenolysis, Diabetes, Fractional order differential, Damped oscillations*

Corresponding author: Vaibhab Ghosh *E-mail address:* vaibhabghosh93@gmail.com
Received: April 16, 2026 **Revised:** June 1, 2026 **Accepted:** June 13, 2026 **Published:** June 14, 2026
 DOI: 10.67029/j.amb.2026.0021.17

1. Introduction

Since the beginning of the 21st century, diabetes has emerged as one of the most prevalent non-communicable diseases (NCDs). It is a complex metabolic disorder driven by multi-factorial impairments and high-carbohydrate diets [1]. According to the International Diabetes Federation, approximately 11% of the global population was living with diabetes in 2024, a figure projected to exceed 900 million by 2050 [2]. Consequently, the scientific community has studied this pathology extensively, yet new facets of the disease continue to be discovered. Mathematical modeling has become an indispensable component of this analytical effort.

The glucose-insulin (GI) interaction represents a cornerstone of mathematical modeling in this field. It facilitates an understanding of glucose metabolic pathways, enabling the reproduction of experimental results and enhancing the theoretical framework of glucose uptake networks [3]. The first seminal model in the GI-interaction domain was developed by Bolie (1961) as a "minimal model" [4]. Subsequently, Grodsky (1972) introduced a model capable of exhibiting complex insulin secretion patterns in β-cells—a significant advancement that provided a new pathway for modeling realistic insulin dynamics [5]. A vast corpus of literature now exists regarding the dynamics of biochemical reactions centered on GI-interaction. Critical reviews by Ajmera *et al.* (2013) [6] and Mari *et al.* (2020) [3] provide a comprehensive trajectory of these studies from 1959 to the modern era.

Recent research has become increasingly sophisticated, realistically incorporating the pathophysiology associated with impaired GI-homeostasis. These studies have creatively integrated factors such as diabetic cardiomyopathy, β-cell attrition, and genetic predisposition to analyze glucose homeostasis and potential mitigation strategies beyond metformin. For instance, Boutayeb *et al.* (2014) analyzed impaired β-cell dynamics, offering a novel perspective by identifying genetic predisposition as a primary driver of diabetes [7].

Similarly, Das *et al.* (2020) incorporated cardiac calcium handling and the transport delay of plasma glucose via the insulin-dependent transporter GLUT4 [8]. This work is particularly significant for its holistic overview of treatment strategies for diabetic cardiomyopathy. Further targeting cardiac arrhythmia,

Halder *et al.* (2024) presented a stochastic model that incorporates randomness in GLUT4 translocation, allowing for system analysis within a fuzzy environment [9]. By utilizing Gaussian white noise, this approach elucidates the intricate aspects of arrhythmia associated with impaired glucose homeostasis. Notably, this model explicitly incorporates the GLUT4 translocation system, strengthening its applicability to therapies for insulin resistance. Related studies have explored the restoration of calcium dynamics under diabetic conditions [10] and the importance of excitatory (EC) and non-excitatory (NEC) gap junctional coupling [11], suggesting that functional reductions in gap junctions can induce abnormalities in NEC calcium dynamics.

Beyond cardiac complications, the specific pathways leading to diabetes remain a vital area of contemporary research. Paul *et al.* (2022) developed a minimal model for glucose-stimulated insulin secretion to explore these potential pathways [12]. Additionally, the role of delays in ATP-dependent calcium inflow was observed in [13], exploring recovery pathways for β-cell calcium homeostasis. Metabolic characteristics and the impact of reactive oxidative species (ROS) on β-cell failure have also been critically examined [14].

Historically, ordinary differential equation (ODE) models have been the standard for studying GI-interactions. However, ODEs calculate the next state $(n+1)$ based solely on the current iteration (n). Because the progression of diabetes depends on long-term metabolic impairment—including sustained hyperglycemia and years of dietary habits—these "memoryless" models often fail to capture the cumulative nature of the disease. Consequently, the current state-of-the-art utilizes memory-dependent fractional-order differential equation (FODE) models. FODEs rely on a "memory effect," where the state at $n+1$ is determined by the entire history of the system from the initial state (t_0) to the current iteration (n). This makes FODE models inherently more realistic for analyzing the long-term features of the diabetic state.

Recent literature suggests that FODE models yield results that more closely align with biological reality [15]. As a result, they are increasingly applied to memory-based phenomena in ecology, enzyme kinetics, and viral growth. Notable recent works include Niser *et al.* (2025), who utilized proportional-integral-derivative (PID) control within a GI-dynamic framework [16], and Saber *et al.* (2025), who identified chaos and defined robust methods for analyzing memory-dependent systems [17]. Additionally, Caponetto *et al.* (2024) analyzed the Bergman minimal model for Type-1 diabetes through the lens of β-cell mass [18]. While these studies [19–21] have advanced the field, the existing literature lacks a model for the complete glucose metabolism network.

The metabolic pathway of glucose is a sophisticated network involving intermediate states and isomers such as glycogen, which serves as a critical ATP reserve. The interplay between fatty-acid metabolism and glycogenesis is fundamental to systemic regulation. Accordingly, the present study introduces a FODE model that integrates GI-dynamics with the glycogenesis network and glucagon dynamics. This intricate interplay accounts for rising plasma glucose triggering insulin release and low glucose levels triggering glucagon-mediated glucose production. This study demonstrates that the fractional order (α) plays a pivotal role in governing system dynamics, with intermediate values producing physiologically consistent outcomes. By analyzing variations in key parameters, such as fasting glucose and dietary intake, this framework highlights the importance of memory-dependent modeling in capturing long-term metabolic behavior and the progression of diabetes.

2. Model development

To develop a fractional order model, it is important to define the fractional order differentiation. Hence, in this study, the Caputo's fractional order differentiation has been incorporated.

Definition 1 *The integration of order α for a function $f : \mathbb{R}^+ \to \mathbb{R}$ is defined by,*

$$I^\alpha f(x) = \frac{1}{\Gamma(\alpha)} \int_0^x (x-t)^\alpha f(t)dt,$$

where $\alpha > 0$. Also provided that, the right side is pointwise defined on $\mathbb{R}^+$.

Definition 2 *The fractional order derivative of order $\alpha \in (n-1, n)$ of a continuous function $f : \mathbb{R}^+ \to \mathbb{R}$ is defined as,*

$$D^\alpha f(x) = I^{n-\alpha} D^n f(x),\ D \equiv \frac{d}{dt}$$

Now, the model can be defined for a system of order α differential equations. Let $G(t)$ be the concentration of glucose in bloodstream at any instance t, $I(t)$ be the concentration of insulin in bloodstream secreted by pancreatic β-cells at time t. $X(t)$ be the concentration of glycogen in liver that produces glucose with the help of glucagon at time t and $P(t)$ be the concentration of glucagon secreted by pancreatic α-cells at time t.

The fasting glucose level has been considered as the basal value of glucose concentration in the bloodstream, is denoted by k_1. The dietary glucose spike in the plasma has been modeled as k_2G. Additionally, the glucagon-glycogen interaction is responsible for the added glucose concentration in the blood stream, which is denoted by k_3XP. The insulin induced glucose uptake has been defined by k_4GI and finally k_5G represents the natural uptake of glucose in bloodstream. Thus the change in the concentration of glucose in bloodstream is represented mathematically by,

$$D^\alpha G = k_1 + k_2G + k_3XP - k_4GI - k_5G.$$

As the glucose concentration rises in the bloodstream, the pancreatic β-cells release insulin to reduce the plasma glucose concentration. This phenomenon is known as glucose induced insulin secretion which has been modeled as k_6G. Additionally, there is an independent insulin secretion by pancreatic β-cells in the blood plasma, which is known as glucose independent insulin secretion [22]. It is defined by k_7I. The insulin secretion is also a self regulatory process, which lowers the amount of glucose induced insulin secretion as a response to the diminished plasma glucose levels. This process has been modeled as k_4GI, which dynamically lowers the insulin concentration [23]. Finally, the natural decay of insulin in the blood plasma has been considered as k_8I.

$$D^\alpha I = k_6G + k_7I - k_4GI - k_8I.$$

As it is mentioned earlier that, glycogen acts as the emergency glucose reserves of the body. Inside the liver, glycogen has been stored through glucose-insulin isomerism pathway. The elevated glucose concentration in the blood plasma triggers the insulin secretion, which converts glucose to its isomer glycogen. This concentration of glycogen has been modeled as k_4GI. When the bloodstream glucose level is very low then pancreatic α-cells release glucagon that interact with glycogen and produce glucose [24], which is modeled as k_3XP, as in glucose concentration. Finally, a glycogen metabolism half-life exists and it has been considered as the glycogen deactivation in the liver [25]. This

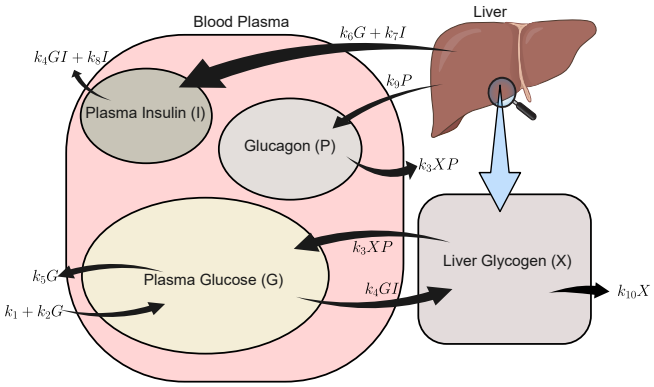

Figure 1. This figure depicts the schematic diagram of the model. Black arrows represents the respective fluxes and the concentration has been presented alongside.

phenomenon has been modeled as $k_{10}X$. Thus the dynamics in the concentration of glycogen in liver is represented mathematically by

$$D^\alpha X = k_4GI - k_3XP - k_{10}X.$$

Glucagon in bloodstream is secreted by pancreatic α-cells, when concentration of glucose in bloodstream is very low, which has been modeled as k_9P, and concentration of glucagon decreases as stated in dynamics of glycogen concentration above which is modeled by the term k_3XP [26]. Thus the change in the concentration of glycogen in liver is represented mathematically by,

$$D^\alpha P = k_9P - k_3XP.$$

Therefore, incorporating the above assumptions the final mathematical model takes the form,

$$\begin{aligned} D^\alpha G &= k_1 + k_2G + k_3XP - k_4GI - k_5G, \\ D^\alpha I &= k_6G + k_7I - k_4GI - k_8I, \\ D^\alpha X &= k_4GI - k_3XP - k_{10}X, \\ D^\alpha P &= k_9P - k_3XP, \end{aligned} \tag{1}$$

with all parameter values and initial states being positive (see the schematic diagram on Fig. 1). Following the work of Ding *et al.* 2006, the fractional order was restricted to $0.5 < \alpha \leq 1$.

3. Analytical results:

Let us denote $\mathbb{R}^4_+ = \{(G,I,X,P) \in \mathbb{R}^4 : G \geq 0, I \geq 0, X \geq 0, \text{and } P \geq 0\}$. Therefore, for any $x \in \mathbb{R}^4_+$ the system can be denoted as,

$$D^\alpha x = F(x),$$

where $F : \mathbb{R}^4_+ \to \mathbb{R}^4$. Now, to prove the solution of the system is unique and non-negative, use the following Lemma.

Lemma 1 (Generalized mean value theorem [27]) *Suppose that $f(x) \in \mathcal{C}[a,b]$ and $D^\alpha_a f(x) \in \mathcal{C}(a,b]$, for $0 \leq \alpha \leq 1$. Therefore, from the Generalized mean value theorem,*

$$f(x) = f(a) + \frac{1}{\Gamma(\alpha)} D^\alpha_a(\xi)(x-a)^\alpha,$$

where $a \leq \xi \leq x$, $\forall x \in (a,b]$.

Corollary 1 *Suppose $f(x) \in \mathcal{C}[a,b]$ and $D^\alpha_a f(x) \in \mathcal{C}(a,b]$, for $0 < \alpha \leq 1$. If $D^\alpha_a f(x) \geq 0, \forall x \in (a,b)$, then $f(x)$ is non-decreasing for each $x \in [a,b]$. If $D^\alpha_a f(x) \leq 0, \forall x \in (a,b)$, then $f(x)$ is non-increasing for each $x \in [a,b]$.*

Proof 1 *The proof follows from over from Lemma 1 [28].*

Theorem 1 (Existence of unique positive and bounded solution) *The solution of the system (1) exists in $\mathbb{R}^4_+$ uniquely for $t \geq 0$ and the solution is also bounded.*

Proof 2 *First, let us define:*$F(G,I,X,P) =$

$$\begin{pmatrix} k_1 + k_2G + k_3XP - k_4GI - k_5G \\ k_6G + k_7I - k_4GI - k_8I \\ k_4GI - k_3XP - k_{10}X \\ k_9P - k_3XP \end{pmatrix}.$$

Since F consists of polynomial functions of the state variables (G,I,X,P), it is continuously differentiable on $\mathbb{R}^4_+$. Hence, F is locally Lipschitz continuous. Therefore, by the standard existence and uniqueness theorem for Caputo's fractional differential equations, for every initial condition $(G(0),I(0),X(0),P(0)) \in \mathbb{R}^4_+$, system (1) admits a unique local solution. Again at the boundary of $\mathbb{R}^+$ we have each $D^\alpha G\Big|_{G=0} \geq 0$, $D^\alpha I\Big|_{I=0} \geq 0$, $D^\alpha X\Big|_{X=0} \geq 0$, and $D^\alpha P\Big|_{P=0} = 0$. Thus, on each boundary hyperplane the vector field points inward or is tangent to the boundary. By Corollary 1, solutions initiating in $\mathbb{R}^4_+$ remains inside $\mathbb{R}^4_+$ for all $t \geq 0$. Now, To establish boundedness, let us define:

$$W(t) = G(t) + I(t) + X(t) + P(t).$$

Therefore, from system (1), we have:

$$\begin{aligned} D^\alpha W = k_1 + (k_2 - k_5 + k_6)G + (k_7 - k_8)I - k_{10}X \\ + k_9P - k_3XP. \end{aligned}$$

Since $X, P \geq 0$, it follows that $-k_3XP \leq 0$. Again let $M = \max\{k_2 - k_5 + k_6,\ k_7 - k_8,\ k_9\}$. Then

$$D^\alpha W \leq k_1 + MW.$$

Applying the fractional Grönwall inequality yields:

$$W(t) \leq \left(W(0) + \frac{k_1}{M}\right) E_\alpha(Mt^\alpha) - \frac{k_1}{M},$$

where $E_\alpha(\cdot)$ denotes the Mittag–Leffler function. Therefore, $W(t)$ remains finite for every finite $t \geq 0$. Since all state variables are non-negative and satisfy:

$$0 \leq G(t),\ I(t),\ X(t),\ P(t) \leq W(t)$$

, consequently, each component of the solution is bounded. Hence, the unique solution of system (1) exists globally for all $t \geq 0$, remains non-negative, and is bounded in R^4_+. This completes the proof [28, 29].

Now proceed to the stability analysis of the system (1). To obtain the equilibrium of the system (1), let us put,

$$\begin{aligned} D^\alpha G &= 0, \\ D^\alpha I &= 0, \\ D^\alpha X &= 0, \\ D^\alpha P &= 0. \end{aligned}$$

Since the system conveys physiological significance, an interior equilibrium point is of interest in this analysis. The system

contains a physiological steady-state (internal equilibrium point) described as $E^* \equiv (G^*, I^*, X^*, P^*)$, provided $k_5 - k_2$, $kk_9k_{10} - k_1k_3$ have the same sign, and $k_1k_3 - k_9k_{10}$ and $\hat{k}$ have the same sign, where $\hat{k} = k_1k_3k_4 + k_2k_3k_7 - k_3k_5k_7 - k_2k_3k_8 - k_4k_9k_{10}$. The steady-state values are given by,

$$G^* = \frac{k_{10}k_9 - k_1k_3}{k_3(k_2 - k_5)},$$
$$I^* = \frac{k_6(k_1k_3 - k_{10}k_9)}{\hat{k}},$$
$$X^* = \frac{k_9}{k_3},$$
$$P^* = \frac{k_4}{k_9}G^*I^* + \frac{k_{10}}{k_3}.$$

At the general equilibrium point $E^* \equiv (G^*, I^*, X^*, P^*)$, the Jacobian matrix have been calculated as, $J(G^*, I^*, X^*, P^*) =$

$$\begin{bmatrix} k_2 - k_5 - a & -b & c & d \\ k_6 - a & k_7 - k_8 - b & 0 & 0 \\ a & b & -c - k_{10} & -d \\ 0 & 0 & -c & k_9 - d \end{bmatrix}$$

where $a = k_4I^*$, $b = k_4G^*$, $c = k_3P^*$, and $d = k_3X^*$. The qualitative nature of the system has been summarized through the following theorem,

Theorem 2 *The general condition for the physiological steady-state E^* to be stable, if the eigenvalues (λ) of the corresponding Jacobian matrix ($J(E^*)$) satisfies the following condition, $|\arg(\lambda)| > \frac{\alpha\pi}{2}$.*

Theorem 3 *The necessary conditions for the physiological steady-state E^* is to be locally, asymptotically stable for $\alpha \in (0, 1]$ is given by, $A_1 > 0$, $A_4 > 0$, $A_1A_2 - A_3 > 0$, $A_1A_2A_3 - A_3^2 - A_1^2A_4 > 0$, and the discriminant of $p(\lambda) = 0$, denoted by $\mathbf{D}(p)$ should be positive, means $\mathbf{D}(p) > 0$.*

Proof 3 *First take the Jacobian matrix for the physiological steady-state, that has been calculated as $J(E^*)$. Then take a general characteristic polynomial of $J(E^*)$ as,*

$$p(\lambda) \equiv \lambda^4 + A_1\lambda^3 + A_2\lambda^2 + A_3\lambda + A_4 = 0, \tag{2}$$

Therefore the first three conditions can be proved from Routh-Hurwitz criterion [30]. Now for the fourth condition, take the discriminant of characteristic polynomial (2) from the Sylvester's matrix for $p(\lambda)$ and $p'(\lambda)$ as: $\mathbf{D}(p) =$

$$\begin{vmatrix} 1 & A_1 & A_2 & A_3 & A_4 & 0 & 0 \\ 0 & 1 & A_1 & A_2 & A_3 & A_4 & 0 \\ 0 & 0 & 1 & A_1 & A_2 & A_3 & A_4 \\ 4 & 3A_1 & 2A_2 & A_3 & 0 & 0 & 0 \\ 0 & 4 & 3A_1 & 2A_2 & A_3 & 0 & 0 \\ 0 & 0 & 4 & 3A_1 & 2A_2 & A_3 & 0 \\ 0 & 0 & 0 & 4 & 3A_1 & 2A_2 & A_3 \end{vmatrix},$$

hence, the necessary condition for local stability of the system (1) is that the discriminant of (2), should satisfy $\mathbf{D}(p) > 0$ [29].

Theorem 4 *If the discriminant of $p(\lambda) = 0 : \mathbf{D}(p) < 0$, then the stability conditions corresponding to the equilibrium (E^*) is given by, if $A_i \geq 0$ for $i = 1, 2, 3$, and $A_4 > 0$, then E^* is locally, asymptotically stable for $\alpha \in (0, \alpha_c)$.*

Proof 4 *Again the proof has been followed from [29].*

Before starting the proof of global stability analysis, let us assume that for each state variable of system (1), the following properties are satisfied:

$$0 < G_{\min} \leq G(t) \leq G_{\max}$$
$$0 < I_{\min} \leq G(t) \leq I_{\max}$$
$$0 < X_{\min} \leq X(t) \leq X_{\max}$$
$$0 < P_{\min} \leq P(t) \leq P_{\max}$$

Now the global behavior of the system (1) will be checked.

Lemma 2 *Let $f(x)$ be a continuously differentiable function. Then for any $x > x_0$,*

$$D_x^\alpha\Big[f(x) - f^* - f^* \ln\frac{f(x)}{f^*}\Big] \leq \Big(1 - \frac{f^*}{f(x)}\Big)D_x^\alpha f(x).$$

Theorem 5 *The interior equilibrium point $E^* \equiv (G^*, I^*, X^*, P^*)$ of system (1) is globally asymptotically stable if $\omega_i < 0$ for i=1, 2, 3, and 4.*

Proof 5 *To prove the global stability of system (1), around interior equilibrium E^*, first consider a Lyapunov function $V(G, I, X, P)$. Since, it is common to consider a Volterra type Lyapunov function for biochemical compartment models, V is given by:*

$$V(G, I, X, P) = c_1(G - G^* - G^* \ln\frac{G}{G^*}) +$$
$$c_2(I - I^* - I^* \ln\frac{I}{I^*}) + c_3(X - X^* - X^* \ln\frac{X}{X^*})$$
$$+ c_4(P - P^* - P^* \ln\frac{P}{P^*}),$$

where c_1, c_2, c_3, and c_4 are positive constants. Then $V(G, I, X, P)$ is a positive definite function and $V(G, I, X, P) = 0$, only at the interior equilibrium point $E^* \equiv (G^*, I^*, X^*, P^*)$. Now taking the α^{th} order derivative of $V(G, I, X, P)$, the value of $D^\alpha V$ is given by:

$$D^\alpha V(G, I, X, P) = c_1D^\alpha(G - G^* - G^* \ln\frac{G}{G^*})$$
$$+ c_2D^\alpha(I - I^* - I^* \ln\frac{I}{I^*}) + c_3D^\alpha(X - X^* - X^* \ln\frac{X}{X^*})$$
$$+ c_4D^\alpha(P - P^* - P^* \ln\frac{P}{P^*}).$$

Using Lemma 2, we have the following inequality:

$$D^\alpha V(G, I, X, P) \leq c_1\Big(1 - \frac{G^*}{G}\Big)D^\alpha G \tag{3}$$
$$+ c_2\Big(1 - \frac{I^*}{I}\Big)D^\alpha I + c_3\Big(1 - \frac{X^*}{X}\Big)D^\alpha X$$
$$+ c_4\Big(1 - \frac{P^*}{P}\Big)D^\alpha P.$$

Substituting the values of $D^\alpha G$, $D^\alpha I$, $D^\alpha X$, and $D^\alpha P$ from (1) at (3), we have:

$$D^\alpha V(G, I, X, P) \leq c_1\Big(1 - \frac{G^*}{G}\Big)\Big[k_1 + k_2G + k_3XP$$
$$- k_4GI - k_5G\Big] + c_2\Big(1 - \frac{I^*}{I}\Big)\Big[k_6G + k_7I - k_4GI$$
$$- k_8I\Big] + c_3\Big(1 - \frac{X^*}{X}\Big)\Big[k_4GI - k_3XP - k_{10}X\Big] +$$
$$c_4\Big(1 - \frac{P^*}{P}\Big)\Big[k_9P - k_3XP\Big].$$

Now using the conditions for the interior equilibrium (G^*, I^*, X^*, P^*) *we have the following inequality:*

$$V(G,I,X,P) \leq V_1(G,I,X,P) + V_2(G,I,X,P) + V_3(G,I,X,P) + V_4(G,I,X,P),$$

where $V_1(G,I,X,P)$, $V_2(G,I,X,P)$, $V_3(G,I,X,P)$ *and* $V_4(G,I,X,P)$ *are given by:*

$$V_1 = c_1\Big(1-\frac{G^*}{G}\Big)\Big[(k_1+k_2G+k_3XP-k_4GI- k_5G)-(k_1+k_2G^*+k_3X^*P^*-k_4G^*I^*-k_5G^*)\Big],$$

$$V_2 = c_2\Big(1-\frac{I^*}{I}\Big)\Big[(k_6G+k_7I-k_4GI-k_8I)- (k_6G^*+k_7I^*-k_4G^*I^*-k_8I^*)\Big],$$

$$V_3 = c_3\Big(1-\frac{X^*}{X}\Big)\Big[(k_4GI-k_3XP-k_{10}X) -(k_4G^*I^*-k_3X^*P^*-k_{10}X^*)\Big],$$

$$V_4 = c_4\Big(1-\frac{P^*}{P}\Big)\Big[(k_9P-k_3XP) -(k_9P^*-k_3X^*P^*)\Big].$$

Therefore, further simplifying the expressions of V_1, V_2, V_3, *and* V_4, *and collecting the coefficients of* $(G-G^*)$, $(I-I^*)$, $(X-X^*)$ *and* $(P-P^*)$, *the expressions become:*

$$V_1 = \frac{c_1}{G}(k_2-k_5-k_4I^*)(G-G^*)^2 + \frac{c_1k_3X}{G}(G-G^*)(P-P^*) + \frac{c_1k_3P^*}{G}(G-G^*)(X-X^*) - c_1k_4(G-G^*)(I-I^*),$$

$$V_2 = \frac{c_2}{I}(k_6-k_4I^*)(G-G^*)(I-I^*)+ \frac{c_2}{I}(k_7-k_8-k_4G)(I-I^*)^2,$$

$$V_3 = \frac{c_3k_4G}{X}(I-I^*)(X-X^*) + \frac{c_3k_4I}{X}(G-G^*)(X-X^*) - \frac{c_3}{X}(k_3P+k_{10})(X-X^*)^2 - \frac{c_3k_3X^*}{X}(X-X^*)(P-P^*),$$

$$V_4 = \frac{c_4}{P}(k_9-k_3X^*)(P-P^*)^2 - c_4k_3(X-X^*)(P-P^*).$$

Therefore, using the boundedness of $G(t)$, $I(t)$, $X(t)$ *and* $P(t)$ *we have the following inequality as:*

$$V(G,I,X,P) \leq \frac{c_1}{G_{\min}}(k_2-k_5-k_4I^*)(G-G^*)^2 + \frac{c_2}{I_{\min}}(k_7-k_8)(I-I^*)^2 - \frac{c_3}{X_{\min}}(k_3P_{\min}+k_{10})(X-X^*)^2 + \frac{c_4}{P_{\min}}(k_9-k_3X^*)(P-P^*)^2 + T_{GI}+T_{GX}+T_{XP}+T_{GP}+T_{IX}, \tag{4}$$

where, the T_{GI}, T_{GX}, T_{XP}, T_{GP} *and* T_{IX} *are given by:*

$$T_{GI} = \frac{c_2}{I_{\min}}(k_6-k_4I^*)(G-G^*)(I-I^*),$$

$$T_{GX} = \left[\frac{c_1k_3P^*}{G_{\min}}+\frac{c_3k_4I_{\max}}{X_{\min}}\right](G-G^*)(I-I^*),$$

$$T_{XP} = c_4k_3(X-X^*)(P-P^*),$$

$$T_{GP} = \frac{c_1k_3X_{\max}}{G_{\min}}(G-G^*)(P-P^*),$$

$$T_{IX} = \frac{c_3k_4G_{\max}}{X_{\min}}(I-I^*)(X-X^*).$$

Therefore, from the modulus form of Young's inequality, there exists sufficiently small positive real numbers ϵ_1, ϵ_2, ϵ_3, ϵ_4 *and* ϵ_5, *such that:*

$$T_{GI} \leq \frac{c_2}{I_{\min}}|k_6-k_4I^*|\left[\frac{\epsilon_1}{2}(G-G^*)^2+\frac{1}{2\epsilon_1}(I-I^*)^2\right],$$

$$T_{GX} \leq \left[\frac{c_1k_3P^*}{G_{\min}}+\frac{c_3k_4I_{\max}}{X_{\min}}\right]\left[\frac{\epsilon_2}{2}(G-G^*)^2+ \frac{1}{2\epsilon_2}(X-X^*)^2\right],$$

$$T_{XP} \leq c_4k_3\left[\frac{\epsilon_3}{2}(X-X^*)^2+\frac{1}{2\epsilon_3}(P-P^*)^2\right],$$

$$T_{GP} \leq \frac{c_1k_3X_{\max}}{G_{\min}}\left[\frac{\epsilon_4}{2}(G-G^*)^2+\frac{1}{2\epsilon_4}(P-P^*)^2\right],$$

$$T_{IX} \leq \frac{c_3k_4G_{\max}}{X_{\min}}\left[\frac{\epsilon_5}{2}(I-I^*)^2+\frac{1}{2\epsilon_5}(X-X^*)^2\right].$$

Substituting the expressions of T_{GI}, T_{GX}, T_{XP}, T_{GP} *and* T_{IX} *at the inequality (4), we have:*

$$D^\alpha V(G,I,X,P) \leq \omega_1(G-G^*)^2+\omega_2(I-I^*)^2 + \omega_3(X-X^*)^2+\omega_4(P-P^*)^2, \tag{5}$$

where, the expressions of ω_i *are given by:*

$$\omega_1 = \frac{c_1}{G_{\min}}(k_2-k_5-k_4I_{\min})+\frac{c_2\epsilon_1}{2I_{\min}}|k_6-k_4I^*| + \frac{\epsilon_2}{2}\left[\frac{c_1k_3P^*}{G_{\min}}+\frac{c_3k_4I_{\max}}{X_{\min}}\right]+\frac{c_1k_3X_{\max}}{G_{\min}},$$

$$\omega_2 = \frac{c_2}{I_{\min}}(k_7-k_8)+\frac{c_2|k_6-k_4I^*|}{2\epsilon_1I_{\min}}+\frac{c_3k_4G_{\max}\epsilon_5}{2X_{\min}},$$

$$\omega_3 = -\frac{c_1}{X_{\min}}(k_3P_{\min}+k_{10})+\frac{1}{2\epsilon_2}\left[\frac{c_1k_3P^*}{G_{\min}} + \frac{c_3k_4I_{\max}}{X_{\min}}\right]+\frac{c_4k_3\epsilon_3}{2}+\frac{c_3k_4G_{\max}}{2\epsilon_5X_{\min}},$$

Table 1. Biological definitions, units, and baseline values of the system parameters. The concentration of metabolic species is expressed in μM, with time measured in minutes. Parameter values were estimated to ensure physiological consistency with established clinical ranges for glucose homeostasis.

Parameters	Descriptions	Values
k_1	Fasting plasma glucose level per unit time	5
k_2	Dietary glucose input into blood plasma	2.9
k_3	Glycogenolysis induced glucose accumulation in blood plasma	0.125
k_4	Insulin induced glucose uptake	0.1
k_5	Natural uptake of glucose in the bloodstream	0.5
k_6	Glucose induced insulin secretion	20
k_7	Insulin dependent insulin secretion	3
k_8	Natural decay of insulin in blood plasma	5
k_9	Glucagon secretion to perform glycogenolysis	18
k_{10}	Glycogen deactivation per unit time in liver	0.09

$$\omega_4 = \frac{c_4}{P_{\min}}(k_9 - k_3X^*) + \frac{c_4k_3}{2\epsilon_3} + \frac{c_1k_3X_{\max}}{2\epsilon_4G_{\min}}.$$

Therefore, for any arbitrary positive coefficient c_1, c_2, c_3, and c_4, the $D^\alpha V(G,I,X,P)$ is negative definite whenever, $\omega_i < 0$ for each i=1, 2, 3, and 4. For simplicity, let us choose c_1=c_3=c_4=1 and $c_2 = \frac{1}{|k_6 - k_4I^*|}$. Hence, the system (1) is globally asymptotically stable, if $\omega_1 < 0$, $\omega_2 < 0$, $\omega_3 < 0$, and $\omega_4 < 0$.

4. Numerical results

To validate the analytical findings and elucidate the intricate dynamical network of the glucose-glycogen metabolic interaction, numerical simulations were performed for system (1). A reliable biomarker is essential for interpreting these simulation results; consequently, this study utilizes the plasma glucose concentration as the primary indicator. A range of 3.9 mmol/l to 6.1 mmol/l is widely accepted as the standard for glycemic normalcy, and although specific thresholds may vary across studies, the current analysis adopts this range to categorize the findings [31, 32]. Furthermore, as the model is a simplified representation and may occasionally deviate from experimental parameter observations, the baseline parameter set (refer to Tab. 1) has been carefully estimated to ensure that the glucose concentrations yield physiologically admissible results.

Parameter values were initially adopted from previously published and physiologically validated studies [33, 34]. These parameters were then systematically refined through a semi-empirical calibration process, involving iterative adjustments based on comparisons between model predictions and known physiological behavior. The final parameter set was selected to ensure agreement with experimentally observed glucose dynamics and established regulatory trends while preserving biological realism.

The baseline parameter set yields physiologically meaningful glucose concentrations, as illustrated in Fig. 2. The fractional order (α) acts as a critical determinant of system behavior, functioning as a proxy for the "memory effect." Mathematically, a lower value of α increases the system's dependence on its historical states, particularly the initial conditions. Our observations indicate that when $\alpha < 0.6$, the system becomes excessively dependent on its initial state, resulting in a strong memory effect that may suppress the underlying biological interplay and inherent system dynamics. Therefore, a physiologically plausible range for the fractional order is considered to be $0.5 \leq \alpha \leq 1$, where $\alpha = 1$ corresponds to the classical integer-order system. Since the model produces the most clinically consistent outputs at $\alpha \approx 0.75$, this value has been adopted as the default for subsequent analyses.

Furthermore, a significant qualitative observation can be made regarding the progression of the disease. Since diabetes is widely recognized as a consequence of long-term lifestyle shifts—specifically the transition toward high-carbohydrate diets and sedentary habits—the model suggests that a proactive improvement in current dietary and activity parameters can facilitate a reversion to a healthier, normoglycemic state.

Beyond the baseline solution, it is essential to characterize the system dynamics in response to parameter variations. In the context of the current model, a parametric shift represents critical behavioral, dietary, or lifestyle alterations, as well as underlying physiological changes. For instance, the basal plasma glucose concentration (k_1) serves as a defining feature of the system, conceptually representing the fasting plasma glucose level. Consequently, a substantially high value of k_1 may signify a pre-diabetic or diabetic state.

To elucidate the system's sensitivity to k_1, the dynamics were first simulated for the integer-order (ordinary) system. A global perspective of the dynamical behavior was obtained through mathematical continuation methods [35]. For the bifurcation parameter k_1, both Hopf (H) and Transcritical (TC) bifurcations were identified. Prior to the Hopf point, the system exhibits oscillatory behavior, which may be considered physiologically inconsistent with steady-state glucose maintenance; however, beyond the H point, the system transitions into stable steady-states. Subsequently, the system encounters a TC point, where a stability exchange occurs between the stable and unstable steady-state branches (refer to Fig. 3).

A critical observation regarding the dynamical behavior of k_1 is the evolution of the stable steady-state for glucose concentration (see Fig. 3). The steady-state initiates within the physiologically normal range (3.9 mmol/l to 6.1 mmol/l) and subsequently follows a linear downward trajectory until reaching the Transcritical (TC) point. Beyond the TC point, the concentration begins to rise, with the trend suggesting a potential departure from the normoglycemic regime.

From a biological perspective, this phenomenon offers a compelling insight. When the basal (fasting) plasma glucose level is significantly below a specific threshold—represented here by the TC point—an increase in this parameter initially drives the stable steady-state toward a lower trajectory. This may imply a reduction in postprandial glucose levels. However, once the threshold (TC point) is crossed, further increases in k_1 induce

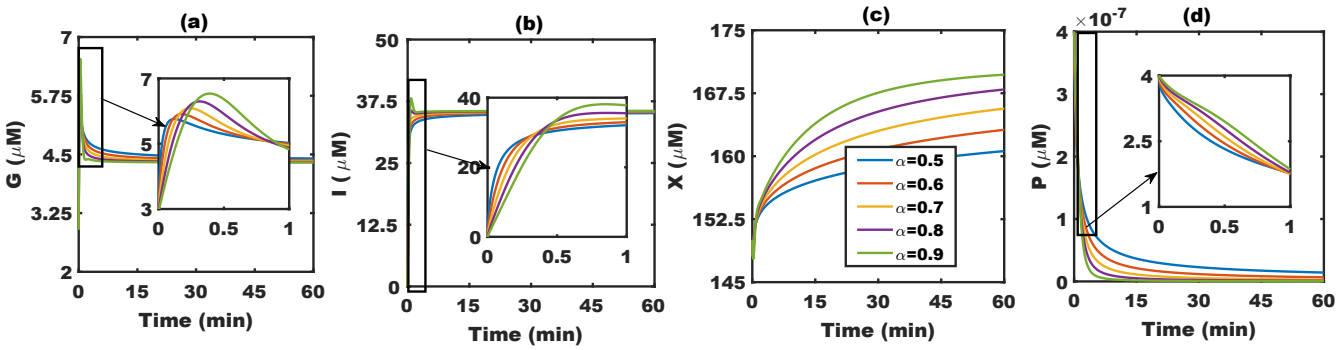

Figure 2. Numerical simulations of glucose concentration for varying α; lower values ($\alpha \in [0.5, 0.75]$) exhibit moderate peaks ($\approx$ 5 mmol/l) and higher steady-states, whereas higher values ($\alpha \geq 0.9$) produce sharp transient peaks ($\approx$ 7 mmol/l) and lower long-term equilibria.

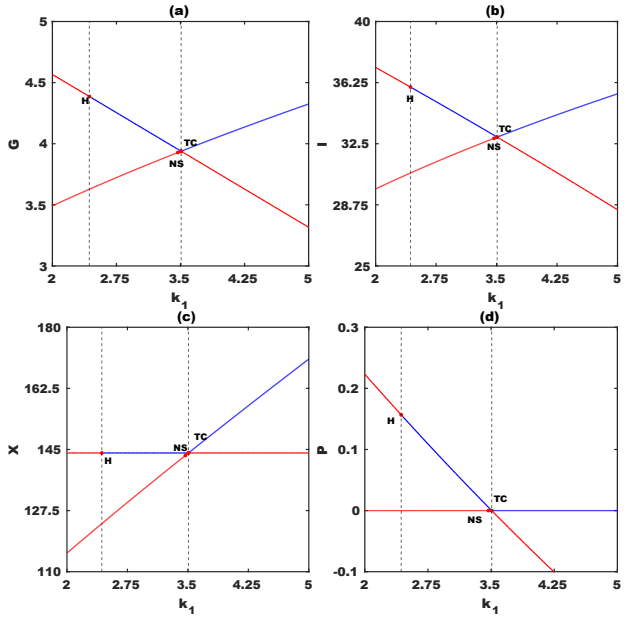

Figure 3. Dynamical behavior and bifurcation analysis of the integer-order system ($\alpha = 1$). The bifurcation diagram for system (1) identifies a Hopf bifurcation (H) at $k_1 = 2.43401$, marking the transition from an oscillatory regime to a stable steady-state. A subsequent Transcritical bifurcation (TC) occurs at $k_1 = 3.50748$, signifying a fundamental shift in steady-state glucose concentrations. Notably, an increase in the basal glucose parameter k_1 correlates with a linear decline in the stable steady-state glucose level. The presence of a neutral saddle (NS) point is also identified within the parametric space.

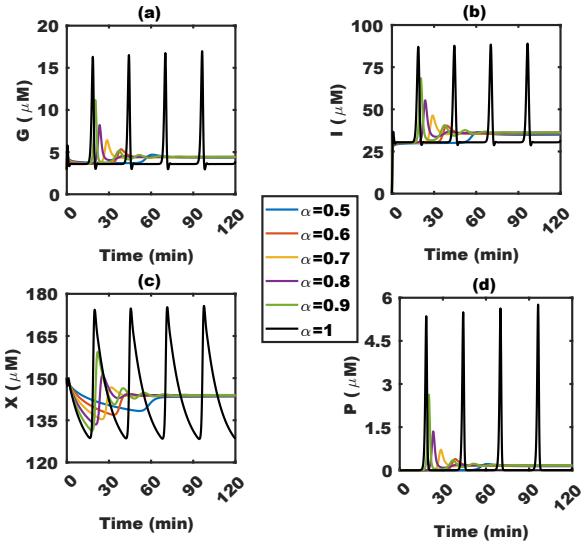

Figure 4. Oscillatory regime and memory-dependent damping. Dynamics of system (1) at $k_1 = 2.3$ with baseline parameters from Tab. 1. For fractional orders $\alpha < 1$, the system exhibits pronounced damping; the intensity of this damping effect is inversely proportional to the value of α. In contrast, the integer-order system ($\alpha = 1$) displays undamped, pure oscillations, effectively eliminating the damping characteristic inherent in the fractional-order framework.

higher glucose concentrations, potentially leading to clinical hyperglycemia. It should be noted that these observations are derived from the integer-order system ($\alpha = 1$); the comparative results for the fractional-order system are presented subsequently in this section.

Given that the integer-order system ($\alpha = 1$) undergoes a Hopf bifurcation, it is essential to explore the system within the oscillatory regime, despite its limited physiological applicability (see Fig. 4). Numerical simulations at $k_1 = 2.3$ reveal that the fractional-order system exhibits damped oscillations for $\alpha < 1$, whereas the integer-order system ($\alpha = 1$) displays nearly undamped oscillatory behavior (Fig. 3). The damping becomes more pronounced as α decreases, highlighting the role of memory effects in stabilizing glucose dynamics and facilitating the return toward physiological steady states. In physiological systems, damped oscillations are significantly more prevalent than undamped, "pure" oscillations. The fact that the incorporation of memory effects naturally induces this characteristic further underscores the biological relevance of the fractional-order framework.

Furthermore, these damped oscillations may fulfill a critical physiological function within the glucose-regulatory network. Following a postprandial glucose spike, the system must stabilize the plasma glucose concentration to maintain homeostasis. The observed damped oscillations facilitate this stabilization, allowing the system to return to a steady state within the normal glycemic range. As the fractional order (α) is varied from 0.5 toward 1, the system becomes increasingly oscillatory, particularly after crossing the threshold of $\alpha = 0.9$. As α approaches unity, the system transitions into a nearly pure oscillatory state, characterized by the absence of discernible damping.

Given that the basal plasma glucose level (k_1) serves as an indicator of significant physiological states, the effects of perturbations on k_1 necessitate detailed investigation within a

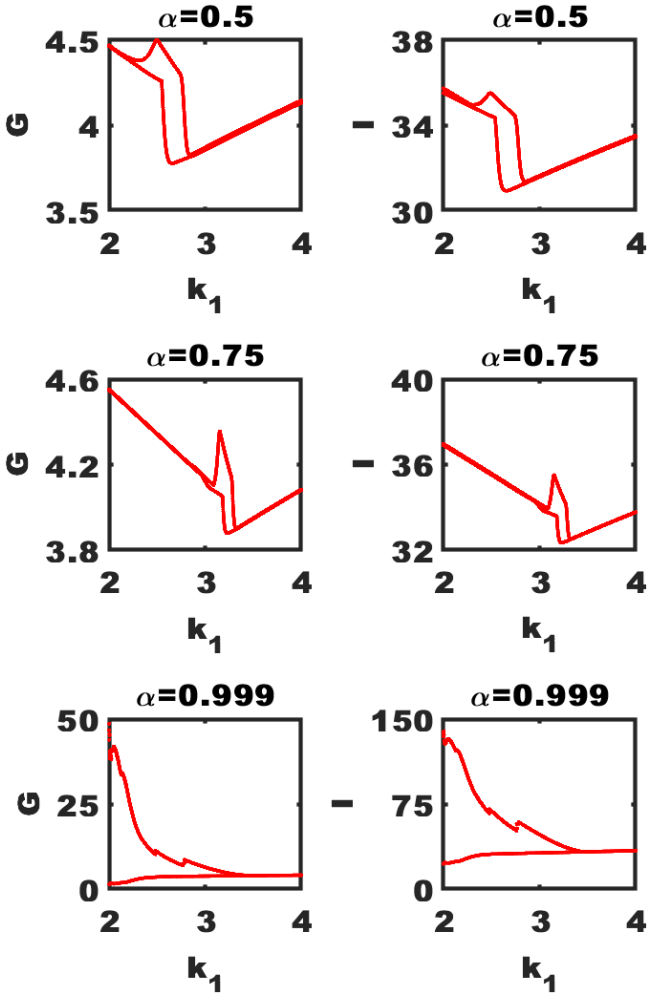

Figure 5. Comparative bifurcation analysis across varying fractional orders. This figure illustrates the distinct dynamical shifts induced by fractional differentiation in contrast to the integer-order system (Fig. 3). Comparative bifurcation structure for varying fractional orders. Lower values of α produce secondary stability regions and damped oscillatory behavior, whereas the dynamics converge toward the integer-order system as $\alpha \to 1$.

fractional-order context. Consequently, bifurcation analysis was performed on k_1 across varying values of the fractional order (α) (see Fig. 5). Under conditions of high memory effects (lower α), the system undergoes two distinct transitions in its dynamical regime. For lower fractional orders, the system undergoes two successive dynamical transitions: a shift from a stable steady-state to a damped oscillatory regime, followed by a return to a secondary stable branch. As $\alpha \to 1$, this secondary stability region gradually disappears, and the dynamics converge toward the single-transition behavior observed in the integer-order system.

In contrast, as the memory effect is reduced (as α approaches 1), the system's behavior increasingly converges with that of the corresponding integer-order (ordinary) system. In this regime, the system exhibits only a single behavioral transition, highlighting the role of the fractional order in introducing secondary stability regions that are absent in traditional ODE models. This analysis further underscores that the incorporation of memory effects yields a system behavior that is significantly more realistic than that of its integer-order counterpart. Consequently, modeling

Table 2. Robustness analysis within the normoglycemic regime. This table delineates the admissible ranges for each system parameter required to maintain the plasma glucose concentration (G) within the physiologically normal interval of 3.9–6.1 mmol/l. During the robustness analysis, each parameter was varied individually while maintaining all other parameters at their baseline values (Tab. 1).

Parameters	Physiological regime
k_1	$0.0045 < k_1 < 16.38$
k_2	$0.0078 < k_2 < 4.524$
k_3	$0.0059 < k_3 < 1200$
k_4	$0.0595 < k_4 < 1200$
k_5	$0.0098 < k_5 < 1900$
k_6	$11.9048 < k_6 < 24$
k_7	$1.785 < k_7 < 3.6$
k_8	$4.167 < k_8 < 7.8$
k_9	$0.005 < k_9 < 1000$
k_{10}	$0.005 < k_{10} < 0.1404$

systems that are intrinsically dependent on long-term historical behavior may benefit substantially from a fractional-order approach. Furthermore, the integer-order (ordinary) system can be conceptualized as a special case within the broader fractional-order continuum, occurring when the memory effect is minimized ($\alpha = 1$).

It is equally imperative to identify the effects of perturbations across the entire parameter space. While the impact of k_1 was detailed in the preceding analysis, other parameters also play crucial roles in maintaining systemic homeostasis. For instance, the dynamics of k_2 are relatively straightforward, as this parameter represents the dietary intake of glucose. Most other parameters exhibit similarly predictable behavior. Consequently, while maintaining the remaining parameters at their baseline values (Tab. 1), the physiologically admissible ranges for the system were explored.

The results of this sensitivity analysis are summarized in the robustness table (see Tab. 2). A notable observation is that the upper bounds for k_3, k_4, k_5, and k_9 are substantially higher than those of the remaining parameters. This suggests that the system exhibits significant robustness against variations in these specific parameters. From a physiological perspective, these parameters represent vital activities within the glucose metabolic network; their robust nature indicates that the system remains fairly consistent and stable despite fluctuations in these underlying physiological conditions. Additionally, the feasible ranges of the system parameters have been identified. Specifically, the admissible parameter intervals are given by $0.00041 < k_1 < 1400$, $0.00081 < k_2 < 1800$, $0.00094 < k_3 < 1200$, $0.00075 < k_4 < 1000$, $0.00048 < k_5 < 1900$, $0.000457 < k_6 < 1200$, $0.00084 < k_7 < 1900$, $0.000411 < k_8 < 1400$, $0.000411 < k_9 < 1000$, $0.00067 < k_{10} < 2400$. Within this parameter regime, the system exhibits admissible dynamics. Furthermore, robustness analysis has been employed to determine the range of physiologically normal behavior associated with these parameter values.

To understand the importance of parameter sensitivity into additional details, it is important to check the standardized sensitivity indices. Hence, a local sensitivity analysis based on standardized sensitivity indices was performed using long-term state-variable dynamics as response metrics (see the results in Tab. 3). For each state variable (G, I, X, P), the root-mean-square (RMS) value over the last half of the simulation

Table 3. Standardized sensitivity indices of the model parameters with respect to the long-term dynamics of glucose (G), insulin (I), glycogen (X), and glucagon (P). The indices were computed using a centered finite-difference scheme with a $\pm 1\%$ perturbation of each parameter and using the RMS value over the final 50% of the simulation interval as the response metric.

Parameters	G	I	X	P
k_1	0	0.0020	0.0112	0.0207
k_2	0	0.0034	0.02746	0.0607
k_3	0	0	0	0
k_4	0	0.0039	0.0059	-0.0045
k_5	0	-0.0006	-0.0047	-0.0104
k_6	0	0.01223	0.0311	0.0344
k_7	0	0.0022	0.0133	0.0222
k_8	0	-0.0037	-0.02221	-0.0372
k_9	0	0	0	0
k_{10}	0	-0.0171	-0.02808	-0.0372

interval was computed to characterize asymptotic behavior while accounting for residual oscillations. Sensitivity indices were then evaluated using centered finite differences under 1% parameter perturbations. Parameters with larger absolute indices were identified as the dominant regulators of long-term metabolic dynamics, whereas parameters with smaller indices indicated increased model robustness.

The sensitivity analysis indicates that the long-term dynamics of the model are primarily influenced by k_6, k_8, and k_{10}. Parameter k_6 exerts the strongest positive effect on insulin, glycogen, and glucagon concentrations, whereas k_8 and k_{10} produce the largest negative effects, highlighting the importance of degradation and depletion mechanisms in regulating metabolic dynamics. Parameters k_2 and k_7 exhibit moderate positive influence, while k_5 has a relatively weak negative effect. The near-zero sensitivity indices associated with k_3 and k_9 suggest that the model is robust to small perturbations in these parameters around the baseline state. Overall, the results identify the key parameters governing the asymptotic behavior of the system and further support the robustness of the proposed fractional-order model.

Through two-parameter space analysis, the interactions between dietary glucose intake (k_2), fasting plasma glucose concentration (k_1), and insulin-induced glucose uptake (k_4) were investigated (refer to Fig. 6). Interestingly, at an intermediate fractional order—specifically when the memory effect is moderate—sudden fluctuations in dietary glucose intake do not impose a discernible impact on the system's stability. However, at the extremes of the studied range, namely under high memory effects ($\alpha = 0.5$) and low memory effects ($\alpha = 0.9$), the system becomes significantly more sensitive to dietary changes.

The global stability of the system was evaluated numerically (refer to Fig. 7). The results demonstrate that, under standard conditions, the solution trajectories converge toward the interior equilibrium point, indicating a robust return to homeostasis. However, a significant deviation occurs at a high memory effect ($\alpha = 0.5$). In this regime, the system fails to satisfy the global stability criteria, manifesting instead as distinct limit cycles and divergent trajectories within the phase space.

This analysis verifies that the system remains within the normoglycemic regime across a variety of initial states. Notably, for an intermediate memory effect ($\alpha = 0.75$), the system consistently yields the most accurate and physiologically

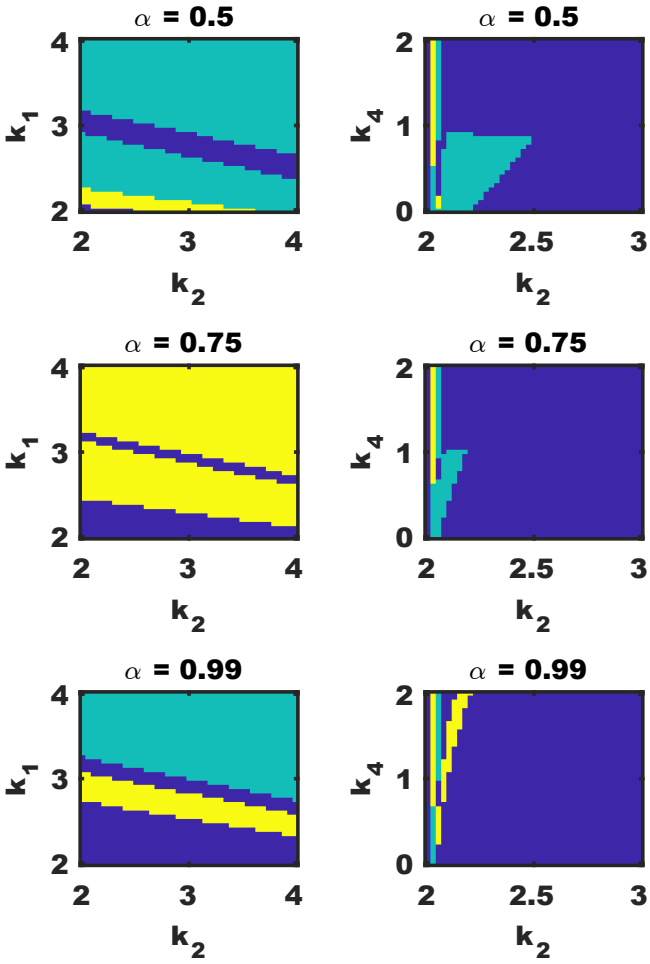

Figure 6. Two-parameter bifurcation analysis in (k_2, k_1) and (k_2, k_4) planes. The stability landscapes illustrate systemic transitions between metabolic states: the blue region represents hypoglycemia ($G < 3.9$ mmol/l), the green region denotes the normoglycemic physiological range ($3.9 \leq G \leq 6.1$ mmol/l), and the yellow region signifies hyperglycemia ($G > 6.1$ mmol/l). The results indicate that both k_1 (basal glucose) and k_4 (insulin-dependent uptake) exhibit high sensitivity to fluctuations in k_2 (dietary intake), suggesting that dietary alterations can trigger rapid departures from the physiological regime.

significant results. This reinforces the finding that moderate fractional orders best capture the balanced regulatory dynamics of the glucose-metabolism network.

5. Discussion

This study characterizes the glucose metabolic pathway by integrating the dynamics of glucose, insulin, glycogen, and glucagon. While fractional-order models are recognized for their ability to incorporate memory effects, a significant gap exists in the literature regarding the integration of comprehensive metabolic networks within this framework. The present model addresses this deficiency by developing a fractional-order representation of the glucose-regulatory metabolic network. Moving beyond classic models that focus exclusively on glucose-insulin interaction, this study incorporates glycogen and glucagon dynamics to provide a more realistic representation of systemic interplay. The inclusion of these variables within a fractional-order framework yields rich dynamical behavior—such as Hopf and Transcritical bifurcations—that aligns more closely with

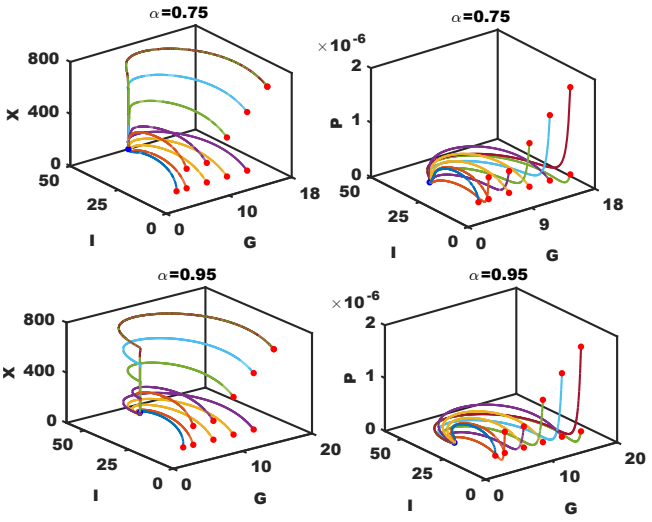

Figure 7. Numerical global stability analysis across various fractional orders. The phase portraits illustrate the convergence of solution trajectories toward the interior equilibrium point for a set of distinct initial conditions. The first row ($\alpha = 0.75$) and the second row ($\alpha = 0.95$) exhibit analogous dynamical behavior, demonstrating robust stability and the system's inherent ability to maintain homeostasis across varying degrees of memory intensity.

biological observations.

The fractional order α represents the system's memory, quantifying the extent to which the current dynamics depend on historical states [36]. For $\alpha = 1$, the model reduces to its classical integer-order form, where the dynamics depend solely on the present state and no memory effects are present. As α decreases from unity, the influence of memory progressively increases, allowing the system to incorporate information from its past states. This feature is particularly relevant in the context of diabetes, whose progression is a long-term process driven by cumulative lifestyle factors, metabolic adaptations, and dietary irregularities rather than abrupt physiological changes [37]. Consequently, the transition toward a diabetic state cannot be adequately captured by memoryless integer-order models.

The threshold $\alpha = 0.5$ is widely regarded as a critical value at which memory effects become sufficiently pronounced while the system retains adequate responsiveness to its present state. Consequently, fractional-order models in molecular biology, physiology, and related biomedical applications are often restricted to the range $\alpha \geq 0.5$, ensuring that hereditary effects are incorporated without allowing the dynamics to become excessively governed by past states [38]. From a biological perspective, this range reflects the fact that cellular and metabolic processes are influenced not only by current conditions but also by accumulated physiological history, including prior glucose exposure, hormonal regulation, and adaptive cellular responses.

Our numerical investigations further reveal that an intermediate fractional order, approximately $\alpha = 0.75$, produces the most physiologically consistent behavior. In this regime, the model successfully balances memory-dependent and instantaneous dynamics, leading to stable convergence toward physiological equilibrium states while accurately reproducing postprandial glucose excursions and recovery patterns. The resulting trajectories closely resemble the expected behavior of a healthy glucose regulatory system, indicating that the chosen fractional order effectively captures the persistence and delayed effects inherent in metabolic regulation [19, 39].

In contrast, when $\alpha < 0.6$, the influence of memory becomes excessively dominant. The system increasingly relies on its historical states, causing a pronounced damping of natural fluctuations and reducing its ability to respond appropriately to changing physiological conditions. As a result, transient responses become unrealistically smooth, and important regulatory variations associated with glucose–insulin interactions are progressively suppressed [40]. Such behavior is inconsistent with experimentally observed metabolic dynamics, where both memory effects and adaptive responsiveness play essential roles.

These observations highlight the importance of selecting an appropriate fractional order when modeling biological systems. The results suggest that diabetes progression and glucose homeostasis are inherently history-dependent processes, influenced by the cumulative effects of previous metabolic states. By explicitly accounting for these hereditary characteristics, fractional-order models provide a more realistic representation of long-term disease dynamics than their classical integer-order counterparts. Therefore, the fractional framework not only improves the physiological interpretation of the model but also offers a valuable tool for investigating disease progression, treatment response, and the long-term regulation of glucose metabolism.

Numerical simulations demonstrate that the fractional-order framework naturally reproduces stable steady states and physiologically realistic damped oscillations. In contrast to the integer-order system, the inclusion of memory effects improves the representation of postprandial stabilization dynamics and long-term glucose regulation.

The present study introduces several key advancements over classical glucose–insulin interaction models. Traditional ordinary differential equation (ODE) frameworks are primarily based on instantaneous system states and often fail to account for the cumulative effects of metabolic dysfunction over time. Although recent research has increasingly adopted fractional-order approaches, many existing models remain limited to minimal glucose–insulin interactions and overlook the broader metabolic network. By incorporating the glycogen–glucagon interplay, the proposed model provides a more comprehensive representation of the glucose regulatory pathway, capturing the complex mechanisms underlying energy storage and mobilization. In addition, the fractional-order formulation successfully reproduces damped oscillatory dynamics, thereby bridging the gap between simplified theoretical descriptions and the physiological complexity of human metabolism. Consequently, the model offers deeper insight into the long-term processes governing glucose homeostasis and metabolic regulation.

Although the present study is not calibrated against a specific clinical dataset, the qualitative behavior predicted by the model is consistent with established experimental observations of glucose regulation. In healthy individuals, postprandial glucose excursions are typically followed by a gradual return toward normoglycemic levels through coordinated insulin secretion and glycogen-mediated metabolic regulation [3]. The proposed fractional-order model reproduces this behavior through transient glucose elevations followed by damped oscillatory relaxation toward a stable equilibrium. Furthermore, the identified sensitivity of the system to fasting glucose levels and dietary glucose intake agrees with clinical and physiological evidence that persistent elevations in basal glucose and excessive carbohydrate consumption contribute to impaired glucose homeostasis and

progression toward diabetes [3, 7]. Notably, previous fractional-order glucose–insulin studies have also reported improved agreement with experimentally observed glucose dynamics when memory effects are incorporated into the mathematical framework [19, 20]. These qualitative agreements support the physiological relevance of the model and suggest that the incorporation of memory effects may provide a realistic framework for describing long-term metabolic regulation.

Our findings carry important physiological implications for glucose regulation. Specifically, the fasting plasma glucose parameter (k_1) emerges as a robust indicator of transitions toward pre-diabetic or diabetic conditions. The model also highlights the profound influence of dietary glucose consumption (k_2); even minimal variations in k_2 can significantly alter system behavior and drive the system beyond the normoglycemic regime. These observations, may reinforce the understanding that sustained lifestyle factors are central to maintaining homeostasis. Moreover, the presence of memory effects suggests that a patient's current metabolic state is shaped by their history, emphasizing the necessity of sustained clinical interventions over short-term corrections.

Despite these advancements, certain limitations must be acknowledged. First, the current study is primarily theoretical and lacks patient-specific clinical data and parameter fitting, which limits the immediate clinical applicability of the findings. Additionally, this study is intended as a qualitative framework to explore the long term metabolic behavior of glucose-insulin regulatory network. Second, the model utilizes simplified linear and bilinear terms, such as k_4GI and k_3XP, whereas biochemical pathways are often highly non-linear and multi-factorial. Future research would benefit from the integration of clinical datasets—incorporating age, genetics, and lifestyle history—to validate these theoretical findings. Expanding the model to include these personalized factors will be essential for advancing the clinical utility of fractional-order metabolic modeling.

6. Conclusion

This study develops a fractional-order glucose metabolism model incorporating glucose, insulin, glycogen, and glucagon dynamics to capture memory-dependent metabolic regulation. The model reproduces key behaviors including damped oscillations, stability transitions, and bifurcation phenomena, while demonstrating the critical influence of the fractional order on long-term system dynamics. Compared with classical integer-order approaches, the proposed framework provides a more realistic representation of glucose homeostasis and diabetes progression. These findings support the applicability of fractional-order modeling for studying complex metabolic disorders and provide a foundation for future clinically calibrated investigations.

Declarations

Acknowledgement: The author is deeply indebted to his doctoral supervisor for his insightful remarks and continuous support, which have substantially built and improved this manuscript. Appreciation is also extended to the anonymous reviewers for their helpful suggestions and critical feedback.

Authors' Contributions: Not applicable.

Funding: There is no fund available for this work.

Conflict of Interest: The authors have no conflict of interest.

Use to AI Tools: AI-based tools like Grammerly has been used to check and improve the grammers and readability of this article.

References

[1] Wahidin, M., Achadi, A., Besral, B., Kosen, S., Nadjib, M., Nurwahyuni, A., ... and Kusuma, D. (2024). Projection of diabetes morbidity and mortality till 2045 in Indonesia based on risk factors and NCD prevention and control programs. Scientific reports, 14(1), 5424.

[2] Genitsaridi, I., Salpea, P., Salim, A., Sajjadi, S. F., Tomic, D., James, S., ... and Magliano, D. J. (2026). of the IDF Diabetes Atlas: global, regional, and national diabetes prevalence estimates for 2024 and projections for 2050. The Lancet Diabetes & Endocrinology, 14(2), 149-156.

[3] Mari, A., Tura, A., Grespan, E., and Bizzotto, R. (2020). Mathematical modeling for the physiological and clinical investigation of glucose homeostasis and diabetes. Frontiers in Physiology, 11, 575789.

[4] Bolie, V. W. (1961). Coefficients of normal blood glucose regulation. Journal of applied physiology, 16(5), 783-788.

[5] Grodsky, G. M. (1972). A threshold distribution hypothesis for packet storage of insulin and its mathematical modeling. The Journal of clinical investigation, 51(8), 2047-2059.

[6] Ajmera, I., Swat, M., Laibe, C., Le Novere, N., and Chelliah, V. (2013). The impact of mathematical modeling on the understanding of diabetes and related complications. CPT: pharmacometrics & systems pharmacology, 2(7), 1-14.

[7] Boutayeb, W., Lamlili, M. E., Boutayeb, A., and Derouich, M. (2014). Mathematical modelling and simulation of β-cell mass, insulin and glucose dynamics: Effect of genetic predisposition to diabetes. Journal of Biomedical Science and Engineering, 7(6), 330-342.

[8] Das, P. N., Kumar, A., Bairagi, N., and Chatterjee, S. (2020). Effect of delay in transportation of extracellular glucose into cardiomyocytes under diabetic condition: a study through mathematical model. Journal of Biological Physics, 46(3), 253-281.

[9] Halder, S., Das, P. N., Ghosh, S., Bairagi, N., and Chatterjee, S. (2024). Studying the role of random translocation of glut4 in cardiomyocytes on calcium oscillations. Applied Mathematical Modelling, 125, 599-616.

[10] Das, P. N., Kumar, A., Bairagi, N., and Chatterjee, S. (2017). Restoring calcium homeostasis in diabetic cardiomyocytes: an investigation through mathematical modelling. Molecular BioSystems, 13(10), 2056-2068.

[11] Das, P. N., Mehrotra, P., Mishra, A., and Bairagi, N. (2017). Calcium dynamics in cardiac excitatory and non-excitatory cells and the role of gap junction. Mathematical Biosciences, 289, 51-68.

[12] Paul, A., Das, P. N., and Chatterjee, S. (2022). A minimal model of glucose-stimulated insulin secretion process explores factors responsible for the development of type 2 diabetes. Applied Mathematical Modelling, 108, 408-426.

[13] Das, P. N., Halder, S., Bairagi, N., and Chatterjee, S. (2020). Delay in ATP-dependent calcium inflow may affect insulin secretion from pancreatic beta-cell. Applied Mathematical Modelling, 84, 202-221.

[14] Paul, A., Azhar, S., Das, P. N., Bairagi, N., and Chatterjee, S. (2022). Elucidating the metabolic characteristics of pancreatic β-cells from patients with type 2 diabetes (T2D) using a genome-scale metabolic modeling. Computers in Biology and Medicine, 144, 105365.

[15] Das, P. N. (2025). Comparative analysis of fractional-order and classical ODE models in explaining real-world dynamics. Applied Mathematical Biosystems, 25-31.

[16] Nisar, K. S., and Farman, M. (2025). Investigation of fractional order model for glucose-insulin monitoring with PID and controllability. Scientific Reports, 15(1), 8128.

[17] Saber, S., Solouma, E., Alharb, R. A., and Alalyani, A. (2025). Chaos in fractional-order glucose–insulin models with variable derivatives: insights from the Laplace–Adomian decomposition method and generalized Euler techniques. Fractal and Fractional, 9(3), 149.

[18] Caponetto, R., Graziani, S., Mughal, I. S., Patanè, L., and Sapuppo, F. (2024). Control of fractional order bergman's glucose-insulin minimal model. IFAC-PapersOnLine, 58(12), 101-106.

[19] Ahmed, G. A. (2023). On the fractional-order glucose-insulin interaction. AIMS Mathematics, 8(7), 15824-15843.

[20] Alshehri, M. H., Duraihem, F. Z., Alalyani, A., and Saber, S. (2021). A Caputo (discretization) fractional-order model of glucose-insulin interaction: numerical solution and comparisons with experimental data. Journal of Taibah University for Science, 15(1), 26-36.

[21] Khirsariya, S. R., Rao, S. B., and Hathiwala, G. S. (2024). Investigation of fractional diabetes model involving glucose–insulin alliance scheme: SR Khirsariya et al. International Journal of Dynamics and Control, 12(1), 1-14.

[22] Meier, J. J., and Butler, P. C. (2013). Insulin secretion. Endocrinology Adult and Pediatric: Diabetes Mellitus and Obesity E-Book, 82.

[23] Braun, M., Ramracheya, R., and Rorsman, P. (2012). Autocrine regulation of insulin secretion. Diabetes, Obesity and Metabolism, 14, 143-151.

[24] Lehninger, A. L. (2004). Lehninger Principles of Biochemistry: David L. Nelson, Michael M. Cox. New York: Recording for the Blind & Dyslexic.

[25] Stetten Jr, D., and Stetten, M. R. (1960). Glycogen metabolism. Physiological reviews, 40(3), 505-537.

[26] Brown, A., and Tzanakakis, E. S. (2023). Mathematical modeling clarifies the paracrine roles of insulin and glucagon on the glucose-stimulated hormonal secretion of pancreatic alpha-and beta-cells. Frontiers in Endocrinology, 14, 1212749.

[27] Odibat, Z. M., and Shawagfeh, N. T. (2007). Generalized Taylor's formula. Applied Mathematics and computation, 186(1), 286-293.

[28] Ding, Y., and Ye, H. (2009). A fractional-order differential equation model of HIV infection of CD4+ T-cells. Mathematical and Computer Modelling, 50(3-4), 386-392.

[29] Ahmed, E., and Elgazzar, A. S. (2007). On fractional order differential equations model for nonlocal epidemics. Physica A: Statistical Mechanics and its Applications, 379(2), 607-614.

[30] Hurwitz, A. (1963). Über die Bedingungen, unter welchen eine Gleichung nur Wurzeln mit negativen reellen Teilen besitzt. Springer Books, 533-545.

[31] Sacks, D. B., Arnold, M., Bakris, G. L., Bruns, D. E., Horvath, A. R., Lernmark, Å., ... and Kirkman, M. S. (2023). Guidelines and recommendations for laboratory analysis in the diagnosis and management of diabetes mellitus. Clinical chemistry, 69(8), 808-868.

[32] Care, D. (2024). 2. Diagnosis and classification of diabetes: Standards of care in diabetes—2024. Diabetes Care, 47(Suppl 1), S20-s42.

[33] Holman, R. R., and Turner, R. C. (1981). The basal plasma glucose: a simple relevant index of maturity-onset diabetes. Clinical endocrinology, 14(3), 279-286.

[34] Roser, W., Beckmann, N., Wiesmann, U., and Seelig, J. (1996). Absolute quantification of the hepatic glycogen content in a patient with glycogen storage disease by 13C magnetic resonance spectroscopy. Magnetic resonance imaging, 14(10), 1217-1220.

[35] Dhooge, A., Govaerts, W., and Kuznetsov, Y. A. (2003). MATCONT: a MATLAB package for numerical bifurcation analysis of ODEs. ACM Transactions on Mathematical Software (TOMS), 29(2), 141-164.

[36] He, S., Wang, H., and Sun, K. (2022). Solutions and memory effect of fractional-order chaotic system: A review. Chinese Physics B, 31(6), 060501.

[37] Abel, E. D., Gloyn, A. L., Evans-Molina, C., Joseph, J. J., Misra, S., Pajvani, U. B., ... and Drucker, D. J. (2024). Diabetes mellitus—Progress and opportunities in the evolving epidemic. Cell, 187(15), 3789-3820.

[38] Magin, R. (2004). Fractional calculus in bioengineering, part 1. Critical Reviews™ in Biomedical Engineering, 32(1).

[39] Magin, Richard. "Fractional calculus in bioengineering, part3." Critical Reviews™ in Biomedical Engineering 32.3&4 (2004).

[40] Alhazmi, M., Mirgani, S. M., Aljohani, A. F., and Saber, S. (2025). Numerical simulation of a fractional glucose-insulin model via successive approximation and ABM schemes. AIMS Mathematics, 10(10), 22817-22849.